Particle Pinch in Gyrokinetic Simulations of Closed Field-Line Systems

Sumire Kobayashi* and Barrett N. Rogers†
Department of Physics and Astronomy, Dartmouth College, Hanover, New Hampshire 03755, USA

William Dorland‡
Department of Physics, University of Maryland, College Park, Maryland 20742, USA
(Received 6 October 2010; published 2 December 2010)

Gyrokinetic simulations of small-scale turbulent transport in a closed magnetic field-line plasma geometry are presented. The simulations are potentially applicable to dipolar systems such as the levitated dipole experiment (LDX) [J. Kesner *et al.*, Plasma Phys. Rep. **23**, 742 (1997).] and planetary magnetospheres, as well as simpler systems such as the Z pinch. We report here for the first time the existence of a robust particle (and weaker temperature) pinch regime, in which the particles are transported up the density gradient. The particle pinch is driven by non-MHD entropy-mode turbulence at $k_\perp \rho_i \sim 1$ and particle pinch appears at larger $\eta \equiv L_n/L_T \gtrsim 0.7$, consistent with quasilinear theory. Our results suggest that entropy-mode transport will drive the LDX plasma profiles toward a state with $\eta \sim 0.7$ and pressure gradients that are near marginal ideal MHD interchange-mode stability.

DOI: 10.1103/PhysRevLett.105.235004 PACS numbers: 52.35.Ra, 52.25.Fi, 52.30.Gz, 52.65.Tt

The transport of plasma by turbulent fluctuations plays an important role in nearly all plasma systems. Typically these fluctuations lead to a relaxation of the plasma gradients and a diffusive spreading of the density and temperature profiles away from ideal boundary. A remarkable exception to this occurs in systems with dipolar magnetic fields, such as planetary magnetospheres or more recently the Columbia-MIT levitated dipole fusion experiment (LDX) [1–3]. In these systems the fluctuations appear to drive plasma inward, creating centrally peaked profiles of the density, pressure, and temperature. One hypothesis is that this inward transport results from mixing due to the ideal MHD interchange instability and the tendency of this mixing to force the system toward a marginally MHD-stable state. For low β, the marginal stability condition for the ideal-interchange mode may be written as $pV^\gamma =$ const, where $\gamma = 5/3$ for isotropic compression, p is the plasma pressure, and V is the volume of a flux tube containing a small but fixed amount of magnetic flux. In a dipolar system the condition $BA =$ const leads to a flux-tube area $A \propto r^3$, a flux-tube volume $V \propto r^4$, and a marginally stable $p \propto r^{-4\gamma}$—that is, a strongly peaked pressure profile. The observed density profiles are somewhat less peaked and seem consistent with the condition $nV =$ const or $n \propto r^{-4}$—a result that is also believed to follow naturally from interchange mixing [2]. The density and pressure conditions may be combined with $p = nT$ to yield $T \propto n^{\gamma-1}$, or equivalently $\eta = L_n/L_T = \gamma - 1 = 2/3$, where L_n and L_T and the density and temperature scale lengths. Thus, to summarize, ideal-interchange mode fluctuations are believed to drive the plasma profiles toward a marginally stable state with $pV^\gamma =$ const and $\eta \simeq 2/3$.

We argue here, based on five dimensional gyrokinetic GS2 [4,5] flux-tube simulations, that these same two conditions can plausibly arise not only from ideal MHD interchange-mode activity but from small-scale, non-MHD entropy-mode transport as well. Considering parameter regimes that are ideally stable, we show for the first time that entropy modes can generate robust, radially inward particle transport comparable to the levels observed in LDX. In the non-MHD scenario presented here, the conditions $pV^\gamma =$ const and $\eta \simeq 2/3$ arise from the dependence of the nonlinear transport on the pressure gradient and η. In particular, we show there are two distinct branches of entropy-mode transport depending on whether $\eta > 2/3$ or $\eta < 2/3$. When $\eta > 2/3$, the transport is driven by the temperature gradient; the temperature flux $Q \propto \langle \tilde{T}\tilde{v}_E \rangle$ is positive while the particle flux $\Gamma_{\rm part} \propto \langle \tilde{n}\tilde{v}_E \rangle$ is negative, and the magnitudes of both increase for increasing η. In this regime, the negative particle transport and positive temperature flux will steepen the density gradient relative to the temperature gradient, driving the system back down to $\eta \sim 2/3$. When $\eta < 2/3$, on the other hand, the density gradient is the driver; the particle flux is positive and the temperature flux is negative and the magnitude of both flux increases very steeply with decreasing η—a feature that will prevent η from falling significantly below $\eta = 2/3$. The two branches of the entropy-mode described above seem to originate from the following. Consider the specific entropy $S = p/n^{5/3} = T/n^{2/3}$. Taking derivative in terms of radial direction r, $\frac{1}{S}\frac{dS}{dr} = \frac{2}{3}\frac{1}{L_n} - \frac{1}{L_T}$. Therefore, when $\eta < 2/3$, $\frac{1}{S}\frac{dS}{dr} > 0$, and when $\eta > 2/3$, $\frac{1}{S}\frac{dS}{dr} < 0$. On the other hand, simulations indicate that the nonlinear transport decreases $\frac{1}{S}\frac{dS}{dr}$ when $\eta < 2/3$, and increases $\frac{1}{S}\frac{dS}{dr}$ when $\eta > 2/3$. Hence, the entropy-mode transport tries to remove the gradient of specific entropy, resulting in two unstable branches with different transport characters. Deep within either zone, the transport for fixed η increases with a

steepening of the pressure gradient and is strong enough to plausibly prevent the profiles from penetrating the ideal-interchange unstable region. The notable exception to this, first pointed out in the linear case in [6], is a narrow zone centered on $\eta \simeq 2/3$—a stability "notch"—in which the marginal stability boundary of the entropy-mode approaches (to within roughly 5%) that of the ideal-interchange mode: $pV^\gamma = \text{const}$. Thus, we believe the stability notch with $\eta \simeq 2/3$ and $pV^\gamma = \text{const}$ will act as an attractor for the profiles, thus providing a non-MHD explanation of these conditions that compliments the ideal MHD arguments outlined above.

We focus our study on two limits of the ring dipole system. One limit is a dipolar flux tube with strong parallel variations of the magnetic field, $B_{\max}/B_{\min} \sim 37$, and a high trapped particle fraction $\sqrt{1 - B_{\min}/B_{\max}} \sim 99\%$. The other limit is a flux-tube very close to the ring and is equivalent to a Z-pinch geometry, in which the parallel variations and trapped particles become negligible and the field lines are circular. Given an appropriate normalization of the dipolar case based on outboard midplane parameters, the transport behavior of two systems is qualitatively and quantitatively similar. In particular, the strong negative particle transport observed in the Z-pinch limit for $\eta > 2/3$ shows that trapped particles are not an essential feature of the particle pinch dynamics. The pinch is also robustly insensitive to the value of $\tau = T_e/T_i$ and the plasma collisionalities.

We consider the regime $\beta \ll 1$, in which the dominant instabilities have an electrostatic character and $k_\parallel \ll k_\perp$. There are two kinds of linear instabilities in our system [7]: the ideal MHD interchange-mode and the small-scale non-MHD entropy-mode. The local linear growth rate for the ideal-interchange mode may be written as [7]: $\gamma_{\text{ideal}}/\langle\omega_{di}\rangle_\theta \approx \sqrt{(d - 10/3)/\langle b_i\rangle_\theta}$ where $d \equiv \omega_{*in}(1 + \eta)/\langle\omega_{di}\rangle_\theta = -\frac{dlnp}{dlnU}$ ($d = R/L_p$ for a Z-pinch) is a measure of the pressure gradient, $b_i \equiv (k_\perp^2 T_i/Z_i m_i \Omega_{ci}^2) \ll 1$, $\omega_{*in} \equiv \frac{clT_i}{Z_i e n_0}\frac{dn_0}{d\psi}$ ($\omega_{*i} = k_\perp \rho_i v_{\text{thi}}/L_{n_i}$ for a Z-pinch), $\langle\omega_{di}\rangle_\theta = -\frac{clT_i}{2Z_i eU}\frac{dU}{d\psi}$ ($\omega_{di} = k_\perp \rho_i v_{\text{thi}}/R$ for a Z-pinch; also note our definition of $\langle\omega_{di}\rangle_\theta$ is a factor of 2 smaller tan that of [7]), $\eta \equiv \frac{dlnT_i(\psi)/d\psi}{dlnn_0(\psi)/d\psi} = L_n/L_T$, $\langle\cdots\rangle_\theta = U^{-1}\oint[(\cdots)d\theta/(\mathbf{B}\cdot\nabla\theta)]$, $U(\psi) \equiv \oint[d\theta/(\mathbf{B}\cdot\nabla\theta)]$, ψ is the flux function, n_0 is the background density, and $\oint d\theta$ is an integral along a flux-tube (ignorable in the Z-pinch case). The system is stable to ideal-interchange modes when the gradients are sufficiently weak: $d < 10/3 = 3.33$ for the case of isotropic plasma pressure, and $d < 7/2 = 3.5$ in the CGL (weak-collision) limit. The marginal limit of the former condition ($d = 10/3$) is equivalent to the expression $pV^\gamma = \text{const}$ noted earlier. We focus here exclusively on ideally stable parameter regimes, in which the dominant instability is the entropy mode.

The entropy mode is a plasma analogue of the thermal instability in ordinary fluids [8] modified by magnetic curvature and finite Larmor radius (FLR) effects. As noted earlier, this mode has separate branches for $\eta < 2/3$ and $\eta > 2/3$. In the former case, for a $\tau = 1$ equilibrium, $k_\perp \rho_i \ll 1$, and sufficiently strong collisions, the entropy-mode growth rate is given by [7] $\gamma_{\text{entropy}}/\langle\omega_{di}\rangle_\theta = \sqrt{5/9(d\frac{7-3\eta}{1+\eta} - 10)/(\frac{10}{3} - d)}$. This expression predicts the mode is unstable for $10/7 < d < 10/3$ when $\eta = 0$, while for finite η, stability for any $d < 10/3$ is reached when $\eta > 2/3$. In particular, for $\eta = 2/3$, the marginal stability condition of this branch reduces to $d = 10/3$—the same as that of the ideal-interchange mode. The gyrokinetic simulations, carried out over a range of collisionalities, exhibit a slightly lower entropy-mode threshold (typically by about 5%), as can be seen from the boundary of the stable white region shown in Fig. 3 for $\eta < 2/3$. The stability notch referred to earlier is represented by the upward indentation in the stability boundary near $\eta \simeq 2/3$.

The linear stability of the $\eta > 2/3$ branch of the entropy mode is more complicated; finite $k_\perp \rho_i$ effects can be important and the dispersion relation is high-order polynominal equation in both the low [9] or high [6,7] collision limits. The marginal stability threshold for this branch obtained from the GS2 simulations is represented by the boundary of the stable zone in Fig. 3 for $\eta > 2/3$. Typical linear growth rates are shown in Fig. 1(a) (dipolar case) and Fig. 1(b) (Z-pinch) as a function of $k_\perp \rho_s$. (Here γ is normalized to c_s/R_{mid} where $c_s^2 = (T_i + T_e)/m_i$ and R_{mid} is the distance from the current ring to the outboard midplane of the flux tube, and $\rho_s = c_s/\Omega_{ci}$. Unless otherwise noted, ρ_s and ρ_i for the dipolar case are evaluated at the outer midplane). The difference between the dipole and Z-pinch plots are due in part to the rather extreme choice of an outboard midplane normalization in the former: normalizing γ and $k_\perp$ to the other extreme, the inboard rather than outboard midplane parameters, for example, decreases the normalized growth rates of the dipolar case by about a factor of 4 and shifts the peak of the k spectrum down to $k_\perp \rho_s \sim 1/37 \sim 0.03$.

Turning to the nonlinear regime, our simulations include up to 128×128 Fourier modes in the perpendicular directions spanning $0.13 \le k_\perp \rho_i \le 5.5$ for the dipole case and $0.016 \le k_\perp \rho_i \le 1.3$ for the Z pinch, and 32 grid points in the parallel direction (the Z-pinch system remains uniform

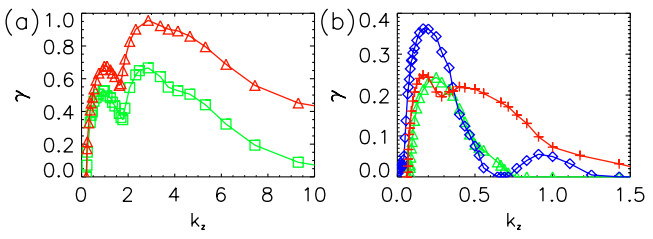

FIG. 1 (color online). γ vs $k_\perp$ in (a) a dipole for $\eta = 2$ (squares) and 4 (triangles) at $d = 3.22$, and $\tau = 1$; (b) a Z pinch for $\tau = 0.5$ (crosses), 1 (triangles), and 10 (diamonds) at $d = 3.2$, and $\eta = 3$.

in the parallel direction). For the ions and electrons we use 24 energy grid points each in the velocity space region $0 \leq v \leq 6v_{\rm thi}$ and 10 grid points in $\xi = v_\parallel/v$. Simulations have been carried out to verify the insensitivity of the transport levels to variations in the spatial and velocity space resolutions and box size. The transport depends only weakly on the mass ratio m_i/m_e; most dipole runs employ a deuterium mass ratio $m_i/m_e = 3672$ (the target for LDX) while the Z-pinch runs use $m_i/m_e = 1836$. The collision frequency is defined as $\nu_{\rm phys} = \pi n_0 e^4 \ln\Lambda/(T_i^{3/2} m_i^{1/2}) \equiv \nu\sqrt{2} v_{\rm thi}/R_{\rm mid}$. Collisions in the code are modeled by a gyro-averaged Lorenz collision operator [9] that conserves total energy and particle number. The simulations presented here have a small base value of $\nu = 0.000015$ for the dipolar geometry and $\nu = 0.001$ for the Z-pinch case. Simulations at higher collisionalities up to $\nu = 0.1$, particularly near marginal entropy-mode stability, can exhibit significantly stronger positive and negative transport levels, due mainly to the collisional damping of zonal flows [10]. In the Z-pinch limit, an artificial hyperviscous term in the gyrokinetic equations is included that acts on the guiding center distribution functions and leads to dissipation proportional to k^4 [11]. No numerical hyperviscosity was used for the dipolar simulations.

The dominant modes contributing to the transport typically have $k_\perp$ values that are 1/4 to 1/2 those of the fastest growing modes shown in Fig. 1. A comprehensive plot of the transport in the Z-pinch case for various d and η is shown in Fig. 2. The first, second, and third figures represent $\Gamma_{\rm part}$, ion temperature flux, and electron temperature flux (normalized to $(\rho_s/R_{\rm mid})^2 c_s f$ with $f = n_0$ for the particle flux and $f = n_0 T_\alpha$ for the temperature flux) for $\tau = 1$ (similar results are obtained for a range of τ, $0.5 \lesssim \tau \lesssim 10$). The blue regions of the left figure in Fig. 2 for $\eta > 2/3$ represent the particle pinch regime. As noted earlier, we would expect the negative particle flux and positive temperature flux typical of the pinch region to drive the system leftward (toward smaller η) in the figures. If the stability boundary (the white region) is encountered during this leftward traverse, the transport would drop and

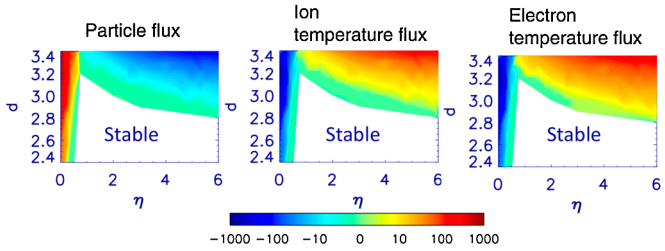

FIG. 2 (color online). Z-pinch transport vs d and η: $\Gamma_{\rm part}$ (left column), ion temperature flux (middle column), electron temperature flux (right column) for $\tau = 1$. Red-yellow areas indicate positive radial transport, and blue-green areas indicates negative (pinched) values. The mode is stable in the white region. The upper boundary of the plots at $d \simeq 3.4$ are just below the ideal MHD instability boundary in GS2.

pressure gradient would steepen, thereby forcing the system upward (toward higher d) and then leftward again, until finally the notch region ($\eta \simeq 2/3$ and marginal MHD stability) is reached. At that point, further decreases in η below 2/3 lead to positive, large, and sharply increasing particle and (pinched) temperature fluxes [10], likely preventing a significant drop in η below 2/3. The transport in the $\eta \simeq 2/3$ region in LDX would likely be due to a mixture of ideal-interchange modes and entropy modes.

The transport in the dipolar case is similar to the Z pinch. Figures 3(a) and 3(b) show the nonlinear particle and temperature flux versus d for $\eta = 2$ (triangles) and 4 (diamonds). Additional simulations have been carried out to verify the presence of a stability notch near $\eta \simeq 2/3$ like that seen in Fig. 3. The similarity between the dipolar and Z-pinch transport in the $\eta < 2/3$ case was established in [10]. The normalized transport levels in the dipolar limit are similar to or somewhat lower than the corresponding levels in the Z pinch, but as in the case of the linear growth rates, this depends on the somewhat arbitrary choice of normalization in the dipolar case: choosing normalizing values that are ~30% closer to the ring boosts the normalized dipole transport by about a factor of ~3, while normalizing to the inner-midplane parameters increases the levels by a factor of ~1400.

Defining $\Gamma_{\rm phys} \equiv n v_{\rm eff}$ and considering deuterium LDX plasma parameters with $T_e \sim T_i \sim 100$ eV, $R_{\rm mid} \sim 0.5$ m, $B_{\rm mid} \sim 0.2T \propto 1/R^3_{\rm mid}$, the quantity $v_{\rm eff}$ may be expressed in terms of the normalized GS2 particle flux $\Gamma_{\rm part}$ plotted in Fig. 3 as $v_{\rm eff} \sim \Gamma_{\rm part} v_{\rm thi} (\rho_i/R_{\rm mid})^2 \sim 10\Gamma_{\rm part} (T_i/100\,{\rm eV})^{3/2} (R/0.5\,{\rm m})^4 \sim 10\Gamma_{\rm part}$, where in the $\eta > 2/3$ regime typically $\Gamma_{\rm part} \sim -10$ or less (equivalently, $D \sim \Gamma_{\rm phys}/n_0' \sim v_{\rm eff} L_n$, where $L_n \sim 0.3$ m). Such levels are roughly comparable to those reported in LDX [2].

Some physics of particle pinch can be understood from fluid equations. At $\eta > 2/3$ region, the dominant terms for the pinched transport originate from the balance of the two terms in the electron density equation, $\frac{\partial n}{\partial t} \sim -\nabla \cdot n\mathbf{v}_{\mathbf{E}}$. Linearizing the equation, and keeping only the dominant terms, $\gamma\tilde{n} \sim -\nabla\cdot(n\frac{\mathbf{b}}{B}\times\nabla\tilde{\phi}) \sim -\nabla\tilde{\phi}\cdot(n\nabla\times\frac{\mathbf{b}}{B}) \sim -in_0\mathbf{k}\cdot\nabla\times(\frac{\mathbf{b}}{B})\tilde{\phi}$. For $\beta \ll 1$ (vacuum field), $\nabla\times\frac{\mathbf{b}}{B} = \frac{2}{B}\mathbf{b}\times\vec{\kappa}_m$, where for Z pinch, $\vec{\kappa}_m = -\frac{\hat{r}}{R}$ and $\omega_{di} = k_\perp\rho_i\frac{v_{\rm thi}}{R} > 0$. Then, $\gamma\tilde{n} \sim -2in_0\omega_{di}(\frac{e\phi}{T_{e0}})$, therefore, $\tilde{n} \propto -\tilde{v}_{Er}$. This π

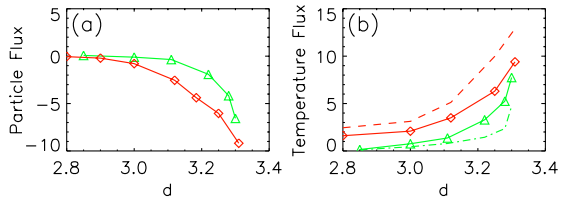

FIG. 3 (color online). (a) $\Gamma_{\rm part}$ for $\eta = 2$ (triangles) and 4 (diamonds) and (b) $Q_{\rm ion}$ (same notation as $\Gamma_{\rm part}$) and $Q_{\rm ele}$ for $\eta = 2$ (green dashed) and 4 (red dashed) vs d for $\tau = 1$ in the dipole.

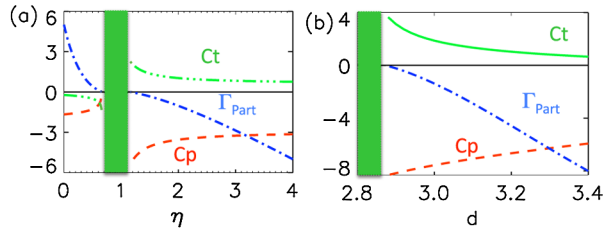

FIG. 4 (color online). Γ_{part}, C_P, and C_T calculated from gyrokinetic quasilinear theory for (a) $d = 3.2$ as a function of η and (b) $\eta = 2$ as a function of d.

phase difference is expected to create the pinched particle flux $\Gamma_{\text{part}} \sim \langle \text{Re}(\tilde{n})\text{Re}(\tilde{v}_{Er})\rangle$. More complicated but similar argument can be made for temperature pinch.

More precise argument can be obtained using gyrokinetic model. The simulations show that the onset of the particle pinch occurs in the linear stage, suggesting that some insight into the physics of the pinch may be gained from quasilinear theory. For simplicity we consider the case of $\tau = 1$ and $\nu = 0$ in the Z-pinch system with isotropic Maxwellian ion and electron equilibrium distribution functions F_0. The particle flux can be written as $\Gamma_{\text{part}} = \langle \text{Re}(\tilde{n})\text{Re}(\tilde{v}_E)\rangle_z = \frac{c}{B}\langle \text{Re}(\tilde{n})\text{Re}(ik_z\tilde{\phi})\rangle_z$ where z represents the usual coordinate parallel to the symmetry axis of the Z pinch. The goal of the calculation is to use the (electron) gyrokinetic equation to relate $\tilde{n}$ to $\tilde{\phi}$. This relationship depends on the mode frequency $\omega = \omega_r + i\gamma$ and it is therefore necessary to use the gyrokinetic equations to first evaluate ω as a function of the parameters d and η. Neglecting electron FLR effects, the perturbed electron distribution function f_e can be written as $f_e = -e\frac{\partial F_{0e}}{\partial \epsilon}\tilde{\phi} + h_e$ where $(\omega - \Omega_{de})h_e = (\omega - \Omega_{*e})e\frac{\partial F_{0e}}{\partial \epsilon}\tilde{\phi}$, $F_{0e} = n_0(\frac{m_e}{2\pi T_{0e}})^{3/2}\exp(-\frac{\epsilon}{T_{0e}})$, $\epsilon = \frac{m_e(v_\parallel{}^2 + v_\perp{}^2)}{2v_{\text{the}}{}^2}$, $\Omega_{*e} = -\omega_{*in}[1 + (\frac{\epsilon}{T_{0e}} - \frac{3}{2})\eta] = -k_\perp\rho_i v_{\text{thi}}/L_n(1 + g\eta)$, $g \equiv \frac{\epsilon}{T_{0e}} - \frac{3}{2}$, $\Omega_{de} = -\omega_{di}(\frac{v_\parallel{}^2 + v_\perp{}^2/2}{v_{\text{the}}{}^2})$. Integrating f_e over velocity space to obtain $\tilde{n}$, noting that the first (adiabatic) term in f_e does not contribute to Γ_{part} when the spacial average over z direction is taken, and assuming $\tilde{\phi} = \tilde{\phi}_0 e^{ik_z z - \omega t}$ for some real ϕ_0, one obtains $\Gamma_{\text{part}} = \text{Im}[\int \frac{\omega - \Omega_{*e}}{\omega - \Omega_{de}}\frac{\partial F_0}{\partial \epsilon} d^3v]k_z\phi_0^2 e^{2\gamma t}\frac{ec}{2B}$. Evaluating the velocity space integral numerically, one finds the sign Γ_{part} agrees well with the GS2 simulations shown in Fig. 2 for both η branches. Following the notation and terminology of [12], Γ_{part} may be decomposed as

$$\Gamma_{\text{part}} = \left(1 + \eta C_T + \frac{1+\eta}{d}C_P\right)\alpha_1\alpha_0 e^{2\gamma t} \qquad (1)$$

where

$$C_T \equiv \frac{1}{\alpha_1}\text{Im}\left[\int \frac{g}{\omega + \Omega_{di}}\frac{\partial F_{0e}}{\partial \epsilon} d^3v\right],$$

$$C_P \equiv \frac{1}{\alpha_1}\text{Im}\left[\int \frac{\omega/\omega_{di}}{\omega + \Omega_{di}}\frac{\partial F_{0e}}{\partial \epsilon} d^3v\right],$$

$$\alpha_1 \equiv \text{Im}\left[\int \frac{1}{\omega + \Omega_{di}}\frac{\partial F_{0e}}{\partial \epsilon} d^3v\right] > 0$$

$$\alpha_0 \equiv \frac{cek_z^2\rho_i v_{\text{thi}}}{2BL_n}\phi_0^2 > 0.$$

and the positivity of α_1 has been established numerically. As can be seen from Eq. (1), a negative value of Γ_{part} is obtained only when C_T and/or C_P are sufficiently large and negative: the dominance of $C_T < 0$ is denoted a thermo-diffusion pinch, while $C_P < 0$ is associated with a curvature pinch. The particle pinch in the present system falls into the latter category. Figures 4(a) and 4(b) demonstrate typical C_T (three-dots-dashed green) and C_P (dashed red) values in the parameter range of interest with $k_\perp\rho_i = 0.2$. The shaded regions are linearly stable. Considering Fig. 4 (a), the quasilinear $\Gamma_{\text{part}} > 0$ (plotted in arbitrary units) when $\eta \lesssim 1$ and $\Gamma_{\text{part}} < 0$ when $\eta \gtrsim 1$, the latter resulting from strongly negative C_P. Figure 4(b) shows the corresponding plots for fixed $\eta = 2$ as a function of d, where again $\Gamma_{\text{part}} < 0$ is due to $C_P < 0$. A particle pinch is also predicted by fluid theory calculations, provided one uses the gyrokinetic values of ω_r and γ.

This research was supported by grants from the U.S. DOE, EPSCoR-CICART, NERSC, and NASA. We thank Dr. P. Ricci and Dr. E. Fable for useful discussions.

*sumire.kobayashi@dartmouth.edu
†barrett.rogers@dartmouth.edu
‡bdorland@umd.edu

[1] J. Kesner *et al.*, Plasma Phys. Rep. **23**, 742 (1997).
[2] A. C. Boxer *et al.*, Nature Phys. **6**, 207 (2010).
[3] D. T. Garnier *et al.*, J. Plasma Phys. **74**, 733 (2008).
[4] M. Kotschenreuther *et al.*, Comput. Phys. Commun. **88**, 128 (1995).
[5] W. Dorland *et al.*, Phys. Rev. Lett. **85**, 5579 (2000).
[6] J. Kesner, Phys. Plasmas **7**, 3837 (2000).
[7] A. Simakov *et al.*, Phys. Plasmas **8**, 4414 (2001).
[8] A. A. Ware, Nucl. Fusion, Suppl., **3**, 869 (1962).
[9] P. Ricci *et al.*, Phys. Plasmas **13**, 062102 (2006).
[10] S. Kobayashi, B. N. Rogers, and W. Dorland, Phys. Rev. Lett. **103**, 055003 (2009).
[11] P. Ricci, B. N. Rogers, and W. Dorland, Phys. Rev. Lett. **97**, 245001 (2006).
[12] E. Fable *et al.*, Plasma Phys. Controlled Fusion **50**, 115005 (2008).